Precise determination of phase relations in pyrolite across the 660 km seismic discontinuity by in-situ X-ray diffraction and quench experiments

Norimasa Nishiyama*, Tetsuo Irifune, Toru Inoue
Geodynamics Research Center, Ehime University, Matsuyama 790-8577, Japan

Jun-ichi Ando
Department of Earth and Planetary Systems Science, Hiroshima University, Higashi-Hiroshima 739-8526, Japan

Ken-ichi Funakoshi
Japan Synchrotron Radiation Research Institute, Mikazuki, Sayo-gun, Hyogo 679-5198, Japan

* corresponding author

Tel.: +81-89-927-8408
Fax: +81-89-927-9640
E-mail: nisiyama@sci.ehime-u.ac.jp

Submitted to Special Issue of Physics of the Earth and Planetary Interiors
February 5th, 2003

Abstract

Mineral assemblage changes in a pyrolite composition with increasing pressure were observed by in-situ X-ray diffraction and some additional quench experiments at pressures near the 660 km seismic discontinuity and at a fixed temperature of 1600°C. Ringwoodite was observed with majorite garnet and $CaSiO_3$-rich perovskite at pressures 20.4-21.3 GPa. Dissociation of ringwoodite to $MgSiO_3$-rich perovskite and magnesiowüstite occurred at 22.0±0.2 GPa, while majorite garnet persisted to about 24 GPa where pyrolite transformed to a lower mantle mineral assemblage, i.e., $MgSiO_3$-perovskite, $CaSiO_3$-rich perovskite, and magnesiowüstite. Thus, majorite garnet coexists with the lower mantle assemblage at pressures of 22-24 GPa. At 22.5 GPa, just above the ringwoodite dissociation pressure, Mg-perovskite contained 2.8 wt% Al_2O_3, and it is significantly poorer in Fe than the coexisting magnesiowüstite. The Fe-Mg partition coefficient between Mg-perovskite and magnesiowüstite including ferric iron (K^{app}) at these P-T conditions is very close to that in the Al-free system at this pressure. Above this pressure, Mg-perovskite becomes richer in Al and Fe with increasing pressure, which supports the present in-situ X-ray observations that demonstrated the transition of garnet to aluminous Mg-perovskite occurs above the ringwoodite dissociation pressure. It is also suggested that $FeAlO_3$ component in Mg-perovskite increases with pressure. The relation between the Al content in Mg-perovskite and K^{app} is non-linear in pyrolite, which is consistent with the Fe-Mg partitioning between Mg-perovskite and magnesiowüstite previously reported for a simpler MgO-FeO-Al_2O_3-SiO_2 system.

1. Introduction

Pyrolite is a hypothetical rock composition first proposed by Ringwood (1966), and has been believed as a compositional representative of the upper mantle. In contrast, there is little direct information about chemical composition of the lower mantle because of the lack of petrologic evidence. Pyrolite is also considered as a potential candidate of the lower mantle material because the calculated density and velocities of pyrolite under lower mantle conditions using experimentally determined equation-of-state parameters of lower mantle minerals are in good agreement with those obtained from seismic observations (e.g. Yagi and Funamori, 1996; Fiquet et al., 1998), although there are some contradictory opinions (e.g. Jeanloz and Knittle, 1989). Detailed studies on the phase relations in pyrolite under the pressure and temperature conditions of the mantle transition zone and the lower mantle are thus crucial to address the composition and dynamics of the entire mantle.

Several attempts have been made to determine the phase relations in pyrolite. Irifune and Ringwood (1987) demonstrated that an assemblage of ringwoodite, majorite garnet, and $CaSiO_3$-rich perovskite is stable in pyrolite at pressures corresponding to the mantle transition zone (15-22 GPa) at a temperature of 1200°C using a Kawai-type apparatus. O'Neill and Jeanloz (1990) extended such experiments using pyrolitic material at pressures corresponding to the deep lower mantle (~54 GPa) using a laser-heated diamond anvil cell, and observed $MgSiO_3$-rich perovskite, magnesiowüstite, and $CaSiO_3$-rich perovskite at these conditions. They confirmed the presence of these phases by X-ray diffraction experiments at high pressure after the sample was quenched to the room temperature. However, the resolution of the X-ray diffraction using a laboratory X-ray source was relatively poor and the chemical analyses of the run products were not made in this study. Irifune (1994) has improved experimental techniques of Kawai-type apparatus to generate higher pressure, and carried out experiments at 28 GPa and 1600°C. He comfirmed the mineral assemblage proposed by O'Neill and Jeanloz (1990) in a pyrolite composition, and determined the chemical

compositions of the coexisting phases. He demonstrated that Mg-perovskite can contain most of Al_2O_3 in pyrolite, and that Al-rich phases proposed by earlier studies (e. g. Takahashi and Ito, 1987) are absent in pyrolite at the lower mantle conditions. Kesson et al. (1998) further extended the pressure range, and studied the phase transitions in pyrolite at pressures of 70 and 135 GPa using a laser-heated diamond anvil cell. They determined chemical composition of the coexisting phases using TEM, and demonstrated that the same phase assemblage as that observed in O'Neill and Jeanloz's and Irifune's study was present in their run products. Therefore it has been well established that pyrolite crystallizes into the ringwoodite-bearing and the perovskite-bearing assemblages at conditions corresponding to the mantle transition zone and the lower mantle, respectively.

Detailed phase changes in pyrolite from ringwoodite-bearing to perovskite-bearing assemblages have been under discussion. Irifune (1994) first proposed that ringwoodite decomposes into $MgSiO_3$-rich perovskite and magnesiowüstite before the garnet transition to the perovskite structure is complete by quench experiments at about 1600°C. Thereafter, Wood (2000) confirmed this result by quench experiments (1627°C) at closely spaced pressure interval, and determined further detailed phase relation and phase chemistry in pyrolite as follows: ringwoodite dissociates into Al-poor $MgSiO_3$-rich perovskite and Fe-rich magnesiowüstite via near-univariant transition; above the transition pressure of ringwoodite, garnet starts to decompose into Ca-perovskite and aluminous $MgSiO_3$-rich perovskite, the latter dissolves into the coexisting Al-poor $MgSiO_3$-rich perovskite produced by the dissociation of ringwoodite. This transition is estimated to be complete within a pressure interval of about 2 GPa. In contrast, Hirose (2002) proposed different phase relations at 1600°C based on quench experiments. According to his results, garnet partially transforms into akimotoite before the dissociation pressure of ringwoodite, and the transition of garnet into the perovskite-bearing assemblage is complete before the end of the ringwoodite dissociation.

In order to clarify the detailed sequence of the mineral assemblage change in pyrolite at the conditions encompassing from the mantle transition zone to the uppermost lower mantle, we performed in-situ X-ray diffraction experiments on pyrolite at pressures of 20-25 GPa and at a fixed temperature of 1600°C. In addition, quench experiments with long heating durations (>12 hours) were carried out at pressures just above the ringwoodite dissociation pressure in pyrolite, and the chemical compositions of the coexisting phases were analyzed carefully. Using a combination of these experimental data, we will examine the detailed phase relations, phase chemistry, and the phase transition pressures in pyrolite under the conditions near the 660 km discontinuity.

2. Experimental

In situ X-ray diffraction experiments were performed at BL04B1, SPring-8. This beam line has a Kawai-type press (SPEED-1500) and X-ray diffraction system for energy dispersive measurements (Utsumi et al., 1998). Incident X-ray from a bending magnet was collimated to form a thin beam (50 μm in horizontal and 300 μm in vertical dimensions) by tungsten carbide slits and directed to the sample via pyrophyllite gasket and magnesia pressure medium. Diffracted X-ray was detected by a pure Ge solid state detector and a 4096-channel analyzer at a fixed diffraction angle of about 6 degrees through a collimator with a 50 μm horizontal slit and additional tungsten carbide slits (200 μm in horizontal and 500 μm in vertical dimensions). The exact diffraction angle was calibrated using d-values of X-ray diffraction peaks of periclase and gold, which were used as pressure markers, at the ambient pressure and temperature.

In order to cover the pressure range of about 25 GPa and to perform in-situ X-ray diffraction experiments for the samples possessing complex chemical compositions, we adopted a newly designed high pressure cell for the second-stage tungsten carbide anvils with truncated edge length (TEL) of 2.5 mm (Fig. 1). Since the anvil gap became narrower in the

present cell as compared to our earlier studies with TEL of 3 mm (Irifune et al., 1998; Kuroda et al., 2000), we placed the sample cylinders horizontally so that the diffraction data of the sample and the pressure markers were able to be easily obtained. In order to avoid kinetic problems, we used synthetic pyrolite as the starting material, which was successfully used in Irifune (1994). A mixture of periclase and gold powders (20:1 in weight) was employed as pressure markers. The starting material and the pressure markers were directly enclosed in semi-sintered MgO sleeves, and molybdenum disks were used to separate each other and to realize homogeneous temperature distributions within these samples. Temperature was measured by a $W_{0.97}Re_{0.03}$-$W_{0.75}Re_{0.25}$ thermocouple without corrections for the effect of pressure on thermocouple-emf.

The cell assembly was first compressed to the target pressure, and then temperature was increased to 1600°C, which is close to the typical temperatures estimated for the 660 km depth (Ito and Katsura, 1989; Brown and Shankland, 1981). This temperature was maintained for about 2 hours under pressure, during which the X-ray diffraction data of the sample and of the pressure markers were collected for 5-10 minutes in about every 30 minutes. We calculated pressures using an equation of state of periclase proposed by Matsui et al. (2000) and that of gold proposed by Anderson et al. (1989). Volume fraction data of these pressure markers and the calculated pressures except those in S141 and S143 were already reported by Matsui and Nishiyama (2002). They demonstrated that the pressures based on Matsui's MgO scale are larger than those derived by Anderson's gold scale by about 1.4 GPa at 1600°C. They argued that this underestimation is due to the lack of electronic thermal pressure in the Anderson's gold scale because it was derived based on the measured elastic and thermodynamic properties of gold at temperatures less than 550 K. However, recent study by Tsuchiya and Kawamura (2001) demonstrated that the effect of electronic thermal pressure in gold is insignificant under such P-T conditions. Nevertheless, we tentatively employed the MgO scale proposed by Matsui et al. (2000), simply because this pressure scale gives us

spinel-postspinel transition pressures which are more consistent with those of 660 km discontinuity, as compared with those based on Anderson's scale of gold. Thus in this study, we avoided the discussion about the absolute values of phase transition pressures, which still have significant uncertainty due to the lack of appropriate pressure scales.

The run was quenched by cutting off the power supply, and then pressure was slowly released. After the decompression, we acquired X-ray diffraction patterns of the run product for about 30 minutes to confirm the phases present at ambient conditions. After this procedure, the recovered sample was polished and examined by an electron microprobe. Neither contamination from the surrounding pressure medium nor the existence of metallic iron were observed in the recovered sample, and the chemical composition analyses using scanning electron beam for wider area (0.5×0.5 mm^2) demonstrated that the bulk composition was unchanged during the high pressure and temperature experiment. The grain sizes of the coexisting phases in the run products especially with $MgSiO_3$-rich perovskite were too small to analyze the chemical compositions of individual phases because of relatively short heating durations (~2 hours). Thus, we performed some additional quench experiments with longer heating durations over 12 hours in order to assure the phase equilibrium and also to enhance the crystal growth of high pressure phases for reliable electron microprobe analyses in pyrolite.

The quench experiments were carried out using a Kawai-type apparatus (Orange-2000) installed at Geodynamics Research Center (GRC), Ehime University. We used a cell assembly with $LaCrO_3$ heater for TEL of 3.0 mm, which is similar to that used in Nishiyama and Yagi (2003). The starting material was the same as that used in the in-situ X-ray diffraction experiments of this study. The sample was put into a gold tube (0.5 mm in ID, 0.7 mm in OD, 0.5 mm in height), which covered by two rhenium disks (0.7 mm in diameter, 0.025 mm in thickness). Temperature was measured by a $W_{0.97}Re_{0.03}$-$W_{0.75}Re_{0.25}$ thermocouple without corrections for the effect of pressure on thermocouple emf. Pressure

calibration at room temperature were performed using semiconductor to metal transitions and its temperature correction was carried out using the dissociation pressure of ringwoodite in pyrolite at 1600°C determined by the present in-situ X-ray diffraction experiments.

The cell assembly was first compressed to the target pressure, and then temperature was increased to 1600°C within 10 minutes. The temperature was maintained for at least 12 hours under pressure. The run was then quenched, and the recovered sample was polished and examined using a micro-focus X-ray diffractometer (MAC, M18XHF) for phase identification. Back-scattered electron image observations and chemical composition analyses of the coexisting phases in the run product were carried out using a scanning electron microprobe with an energy dispersive system (JEOL, JSM-5600) at GRC, Ehime University.

3. Results

Seven in-situ X-ray diffraction experiments were performed at pressures between 20 and 25 GPa and at a fixed temperature of 1600°C, where the press loads were kept constant as in ordinary quench experiments. The phases identified and the calculated pressures based on the X-ray diffraction measurements for each run are listed as a function of run duration in Table 1. In general, pressure slightely (~1 GPa) dropped during the heating, so that the transitions to lower pressure phase assemblages were recognized at later stages in some runs (S136 and S139).

In run S138 (800 tons, 20.4-20.6 GPa), the presence of ringwoodite (Rw), majorite garnet (Gt), and $CaSiO_3$-rich cubic perovskite (CPv or Ca-perovskite) was confirmed (Fig. 2A). This ringwoodite assemblage (Rw+Gt+CPv) did not change throughout the run duration of about 2 hours. The press load was increased to 900 tons in run S136, where the coexistence of ringwoodite and its dissociation products of $MgSiO_3$-rich orthorhombic perovskite (MPv or Mg-perovskite) and magnesiowüstite (Mw) was observed within 20

minutes from the start of temperature retainment. Thus, an assemblage of Rw+MPv+Mw+Gt+CPv, transitional assemblage hereafter, was observed at this heating stage. Upon further heating at this load, pressure dropped to 21.3 GPa, and the complete transition to the ringwoodite assemblage was observed after about 80 minitues. Thus the reverse reaction from the transitional to the ringwoodite assemblage was completed at this pressure.

In run S139 (950 ton), a reverse reaction from the post-ringwoodite assemblage (MPv+Mw+Gt+CPv) to the transitional assemblage was confirmed as pressure decreased from 22.6 to 21.7 GPa after about 1 hour heating (Fig. 2B). The transitional assemblage was maintained upon further heating of 2 hours. In run S110 (1000 tons), the formation of post-ringwoodite assemblage was observed throughout whole heating run duration of about 2 hours, where the pressure ranged from 22.7 to 23.4 GPa. The run duration of 3.5 hours was adopted in S137 (1200 tons), which was significantly longer than those of other experiments. We confirmed the existence of majorite garnet with Mg-perovskite, Ca-perovskite, and magnesiowüstite (Fig. 2C), that is the post-ringwoodite assemblage, from 153 to 206 minutes after the beginning of the temperature retainment. The results of the runs S136, S139, S110, and S137 demonstrated that the boundary between the transitional and the post-ringwoodite assemblage locates between 21.8 and 22.1 GPa. Thus the transition pressure between these assemblages in pyrolite is 22.0±0.2 GPa at 1600°C, when Matsui's MgO scale is adopted.

Majorite garnet persisted to higher pressures as was seen in run S141 (1300 tons, 23.5 GPa), but it finally disappeared at 25.1 GPa in run S143 (1500 tons), as shown in Table 1 and Figure 3. As seen in figure 2C, the diffraction peak of majorite garnet indexed as (420), which should have the maximum intensity in all diffraction peaks of majorite garnet, overlapped with the most intense (110) diffraction peak of Ca-perovskite. Thus we were not able to use this peak of garnet to check whether this phase exists in the run products or not. Nevertheless, we were able to observe these peaks separately at ambient conditions (see Fig. 3A) because of the difference in the compressibilities of these phases: the bulk modulus of

majorite garnet at ambient conditions (160 GPa; Wang et al., 1998) is substantially smaller than that of Ca-perovskite (235±5 GPa; Wang et al., 1996; Shim et al., 2000). At the ambient conditions, we clearly observed the coexistence of Mg- and Ca-perovskite, magnesiowüstite, and garnet (post-ringwoodite assemblage) in the run product recovered from 23.5 GPa, while no diffraction peak of garnet was observed in that recovered from 25.1 GPa (see Fig 3B). This indicates that garnet-to-perovskite transition in pyrolite was complete at a pressure between 23.5 and 25.1 GPa, and that an assemblage of MPv, Mw, and CPv (lower mantle assemblage) was stable above about 25 GPa.

It is well known that $CaSiO_3$-perovskite is unquenchable and amorphizes at the ambient pressure (e.g. Ringwood and Major, 1971). However, we observed X-ray diffraction peaks of Ca-perovskite in recovered samples after the oil pressure was completely released (see fig. 3A, B). Wang et al. (1996) carefully observed this retrograde transformation by in-situ X-ray diffraction measurements, and observed the change of the *P-V* relation during the amorphization processes. If a high-pressure phase is totally quenchable, its unit cell volume should increase with decreasing pressure along the compression curve. However, Wang et al. (1996) observed a marked decrease in the volume of $CaSiO_3$-perovskite when the pressure was lowered from 1GPa to 0.59 GPa. Their observed volume at 0.59 GPa (V=45.22±0.04 Å^3) was close to those of mostly amorphized samples at the ambient conditions (V_0=45.15±0.20 Å^3, Mao et al., 1989; V_0=45.27±0.04 Å^3, Kanzaki et al., 1991). Therefore, Wang et al. (1996) extrapolated the unit cell volumes of $CaSiO_3$-perovskite at high pressures (2-10 GPa) to the room pressure, and determined the unit cell volume at the ambient conditions as V_0=45.58±0.04 Å^3. The unit cell volumes of our Ca-perovskite after the release of pressure were V_0=45.38±0.02 Å^3 (S141) and V_0=45.36±0.03 Å^3 (S143). These values are smaller than the unit cell volume at ambient conditions estimated by Wang et al. (1996), which strongly suggests that Ca-perovskite partially transformed into an amorphous phase in our recovered samples.

Figure 4 summarizes the results of the phase relations in pyrolite at 1600°C as a function of pressure. The ringwoodite assemblage (Rw+Gt+CPv) changes to the post-ringwoodite assemblage (MPv+Mw+Gt+CPv) at 22.0±0.2 GPa via the transitional assemblage, which is limited to a very narrow pressure range (0.3-0.5 GPa). The post-ringwoodite assemblage persists to 24.3±0.8 GPa, above which it transforms into the lower mantle assemblage (MPv+Mw+CPv). The phase boundary between the ringwoodite- and the transitional assemblage, and that between the transitional- and the post-ringwoodite assemblage were drawn assuming that the Clapeyron slopes of these boundaries are the same as that of spinel to postspinel phase boundary in Mg_2SiO_4 (-0.0028 GPa/K; Ito and Takahashi, 1989; Irifune et al., 1998), while the Clapeyron slope of the boundary between post-ringwoodite- and lower mantle assemblage is assumed to be the same as that of the garnet to post-garnet transition in a natural pyrope (0.0065 GPa/K; Oguri et al., 2000).

In order to confirm the results of in-situ X-ray diffraction experiments, some additional quench experiments were carried out at pressures between 22 and 23 GPa, at a temperature of 1600°C. The purpose of these experiments was to synthesize a run product just above the dissociation pressure of ringwoodite in pyrolite, and to measure chemical compositions of the coexisting phases. A sample which meets this purpose was synthesized at 22.5 GPa (OS957), and was carefully examined using a micro-focus X-ray diffractometer to check coexisting phases. This sample was found to comprise Mg- and Ca-perovskite, magnesiowüstite, and garnet (i.e. post-ringwoodite assemblage).

Figure 5 shows a back-scattered electron image of the run product synthesized in OS957. The existence of Mg- and Ca-perovskite, magnesiowüstite, and majorite garnet was confirmed, which is consistent with the observation by a micro-focus X-ray diffraction measurement. Angular gain boundaries in this run product and no chemical zoning in any of these phases suggest that the sample was in equilibrium or at least very close to the equilibrium condtion.

The chemical compositions of Mg-perovskite, magnesiowüstite, and garnet are summarized in Table 2. These values are the averages of ten analyses, and their standard-deviations (σ) are also listed in this table. However, the chemical composition of Ca-perovskite was not measured because of its distinctive aggregate texture (see Fig. 5) with small gains (<1 μm). Garnet contains 8.6 wt% Al_2O_3, which is more majoritic than those synthesized previously in P-T conditions where the post-ringwoodite assemblage is stable in pyrolite (e.g. 20.9 wt% Al_2O_3, Nishiyama and Yagi, 2003). The chemical composition of majorite-garnet synthesized in our experiment is similar to those coexist with ringwoodite in pyrolite at P-T conditions corresponding to the mantle transition zone (e.g. 10.3 wt% Al_2O_3, Irifune, 1994; 8.6 wt% Al_2O_3, Wood, 2000). Existence of the alumina deficient garnet in our run product strongly suggests that our experimental conditions of 22.5 GPa and 1600°C is in the vicinity of ringwoodite dissociation conditions in pyrolite. Actually, the mineral proportions (in volume fraction) in this run product calculated using a mass-balance equation (Irifune et al., 1986) are 46 vol% for Mg-perovskite, 16 vol% for magnesiowüstite, 32 vol% for majorite garnet, and 6 vol% for Ca-perovskite. The proportion of garnet in this recovered sample is very close to that of garnet in a run product synthesized by Irifune (1994) at the mantle transition zone conditions, 56 vol% for ringwoodite, 38 vol% for majorite garnet, and 6 vol% for Ca-perovskite.

4. Discussion

According to our results of both in-situ X-ray diffraction and quench experiments at 1600°C, the sequence of the phase changes in pyrolite with increasing pressure is as follows: ringwoodite assemblage (Rw+Gt+CPv) is stable up to 21.5 GPa, which transforms into the post-ringwoodite assemblage (MPv+Mw+Gt+CPv) at 22.0 GPa via the transitional assemblage (Rw+MPv+Mw+Gt+CPv) with a very narrow pressure range (0.3-0.5 GPa); then the garnet to perovskite transition is complete at 24.3 GPa, where the lower mantle

assemblage (MPv+Mw+CPv) is formed (see Fig.4). This sequence of mineral assemblages in pyrolite is consistent with the results of the previous quench experiments by Irifune (1994), Wood (2000), and Nishiyama and Yagi (2003). In contrast, Hirose (2002) proposed a different sequence of mineral assemblage changes with increasing pressure at 1600°C in pyrolite: garnet partly transforms into akimotoite before the beginning of ringwoodite dissociation, and thus the garnet-to-perovskite transition is complete before the end of ringwoodite dissociation.

The phase relation in pyrolite at pressures above the dissociation of ringwoodite can be further studied by examining the chemical compositions of the coexisting phases. Figure 6 shows the relation between Al-content in Mg-perovskite and K^{app} ($=X_{Fe}^{Pv}X_{Mg}^{Mw} / X_{Mg}^{Pv}X_{Fe}^{Mw}$ where $X_{Fe}^{Pv}= (Fe^{2+}+Fe^{3+})/(Fe^{2+}+Fe^{3+}+Mg^{2+})$) in pyrolite at temperatures of about 1600°C in combination with the results by previous studies (Ito and Takahashi, 1989; Irifune, 1994; Wood, 2000; Nishiyama and Yagi, 2003). A trend that K^{app} increases with increasing Al-content of Mg-perovskite can be seen in this figure. The K^{app} value determined in our run product (0.27±0.06), which was synthesized just above the ringwoodite dissociation pressure, is close to those determined for the Al-free system (~0.14 at 25 GPa and 1600°C; Ito and Takahashi, 1989). This implies that a small amount of Al_2O_3 (<3 wt%) in Mg-perovskite has only a small effect on the Fe-Mg partitioning, whereas a rapid increase of K^{app} with increasing Al_2O_3 content of Mg-perovskite is noted from the results of other studies as depicted in Fig. 6.

The change of K^{app} as a function of the Al-content in Mg-perovskite in pyrolite can be explained by the dissociation of ringwoodite at pressures lower than the garnet-perovskite transition at 1600°C as follows. At pressures corresponding to the mantle transition zone, an assemblage of Rw, Gt, and CPv is stable (Irifune, 1994; Wood, 2000; the results of in-situ X-ray diffraction experiments of our study). Ringwoodite decomposes into low-Al

Mg-perovskite and high-Fe magnesiowüstite at 22 GPa, as determined by in-situ X-ray diffraction experiments. At pressures just above the dissociation of ringwoodite, the partitioning of iron is virtually unchanged until Mg-perovskite becomes to contain about 3 wt% Al_2O_3. With further increasing pressure, garnet dissociates into Ca-perovskite and Al-rich Mg-perovskite, the latter being dissolved into the coexisting Al-deficient Mg-perovskite formed by the dissociation of ringwoodite. Thus the Al-content in Mg-perovskite increases with increasing pressure, which also causes the large increase of iron content in Mg-perovskite via solution of the $Fe^{3+}AlO_3$ component into Mg-perovskite at such high Al concentrations (Frost and Langenhorst, 2002). As a consequence, the Al-content in Mg-perovskite and K^{app} simultaneously increases with increasing pressure as seen in Fig. 6.

This idea that decomposition of ringwoodite and the following garnet transition controls the partitioning of iron between Mg-perovskite and magnesiowüstite in pyrolite was originally proposed by Wood and Rubie (1996), and Wood (2000). The fact that K^{app} of our sample, which was synthesized at conditions just above the dissociation of ringwoodite, is close to those of the Al-free system supports this idea. From Fig. 6, it is obvious that the relation between the Al-content in Mg-perovskite and K^{app} in pyrolite is non-linear. A small amount of Al_2O_3 in Mg-perovskite (less than about 3 wt%) has only a minor effect on the partitioning of iron, whereas the presence of larger amounts of Al_2O_3 in Mg-perovskite affects it considerably.

Therefore, both the results of in-situ X-ray diffraction experiments (Fig. 4) in the present study and the change of K^{app} with increasing pressure (Fig. 6) yield a convergent result that ringwoodite decomposes into Mg-perovskite and magnesiowüstite before the garnet-to-perovskite transition at 1600°C in pyrolite. As mentioned earlier, Hirose (2002) proposed a different sequence of mineral assemblages with increasing pressure at 1600°C in pyrolite: garnet partly transforms into akimotoite before the beginning of ringwoodite dissociation, and thus the garnet-to-perovskite transition is complete before the end of

ringwoodite dissociation. This discrepancy can be explained in terms of difference of starting material (Nishiyama and Yagi, 2003).

A fine-grained reactive mixture formed from a sintered mixture of oxides and carbonates was used by Irifune (1994), Wood (2000), Nishiyama and Yagi (2003), and in the present study, while Hirose (2002) used both finely-ground natural rock powder and a synthesized gel. Irifune (1994) demonstrated that non-equilibrium problems may affect phase relations when rock powders were used as the starting materials, by comparing his results with those of the products synthesized from the natural rock powder (e.g. Takahashi and Ito, 1987). Thus, there is possibility that the results of Hirose (2002) were also affected by similar problems. Actually, in his run products, there are some grains of Al-rich silicate phase, which is probably a residual metastable phase of aluminous spinel that was present in the starting material. The existence of this aluminous phase can cause the apparent aluminum deficiency in his run products, which may be an explanation for the discrepancy between Hirose et al. (2002) and those of four other independent studies (Irifune,1994; Wood, 2000; Nishiyama and Yagi, 2003; this study). The apparent deficiency of aluminum in Hirose's study can cause the transition pressure from majorite garnet to aluminous perovskite to be lower, and the appearance of akimotoite during this transition (Irifune et al., 1996; Kubo and Akaogi, 2000; Hirose et al., 2001).

We observed the non-linear relation between Al-content in Mg-perovskite and K^{app} in pyrolite, which seems to be consistent with the equilibrated Fe-Mg partitioning behavior demonstrated by Frost and Langenhorst (2000) for a simpler MgO-FeO-Al_2O_3-SiO_2 system with careful examination of chemical equilibrium. This consistency in a trend of K^{app} change between the results in a complex system (pyrolite) and the simpler system strongly suggests that the present K^{app} change in pyrolite with increasing pressure is a result of equilibrium reaction in this composition. Therefore, we conclude that the phase relations observed in the studies by Irifune (1994), Wood (2000), Nishiyama and Yagi (2003), and our present study

are applicable to pyrolitic mantle compositions. The resultant density and velocity changes in such compositions with increasing depth actually agree well with those in the representative global seismic models (Irifune, 1994; Wood, 2000).

Acknowledgments

We thank T. Yagi, W. Utsumi, M. Matsui, D. Yamazaki, and O. Shimomura for valuable comments, and K. Kuroda, H. Kageyama, S. Matsushita, K. Kawamura, Y. Higo, M. Nakazawa, T. Sanehira and T. Harada for technical assistance during synchrotron radiation experiments. In-situ X-ray diffraction experiments were carried out at Spring-8 (proposal No. 1999A0102-CD-np). This work was partly supported by the Research Fellowships of the Japan Society for the Promotion of Science for Young Scientists to N. N.

References

Anderson, O. L., Isaak, D. G., Yamamoto, S., 1989. Anharmonicity and the equation of state for gold. J. Appl. Phys. 65, 1534-1543.

Brown, J. M., Shankland, T. J., 1981. Thermodynamic parameters in the Earth as determined from seismic profiles. Geophys. J. R. astr. Soc. 66, 579–596.

Fiquet, G., Andrault, D., Dewaele, A., Charpin, T., Kunz, M., Haüsermann, D., 1998. P-V-T equation of state of $MgSiO_3$ perovskite. Phys. Earth Planet. Inter. 105, 21–31.

Frost, D. J., Langenhorst, F., 2002. The effect of Al_2O_3 on Fe-Mg partitioning between magnesiowüstite and magnesium silicate perovskite. Earth Planet. Sci. Lett. 199, 227–241.

Hirose, K., Fei, Y., Ono, S., Yagi, T., Funakoshi, K., 2001. In situ measurements of the phase transition boundary in $Mg_3Al_2Si_3O_{12}$: implications for the nature of the seismic discontinuities in the Earth's mantle. Earth Planet. Sci. Lett. 184, 567–573.

Hirose, K., 2002. Phase transitions in pyrolitic mantle around 670-km depth: implications for upwelling of plumes from the lower mantle. J. Geophys. Res. 107, 10.1029/2001JB000597.

Irifune, T., Sekine, T., Ringwood, A. E., Hibberson, W. O., 1986. The eclogite-garnetite transformation at high pressure and some geophysical implications. Earth Planet. Sci. Lett. 77, 245–256.

Irifune, T., Ringwood, A. E., 1987. Phase transformations in primitive MORB and pyrolite compositions to 25 GPa and some geophysical implications. in High-Pressure Research in Mineral Physics, edited by M. H. Manghnani and Y. Syono, TERRAPUB, Tokyo, pp231-242.

Irifune, T, 1994. Absence of an aluminous phase in the upper part of the Earth's lower mantle. Nature 370, 131–133.

Irifune, T., Koizumi, T., Ando, J., 1996. An experimental study of the garnet–perovskite

transformation in the system $MgSiO_3$–$Mg_3Al_2Si_3O_{12}$. Phys. Earth Planet. Inter. 96, 147–157.

Irifune, T., Nishiyama, N., Kuroda, K., Inoue, T., Isshiki, M., Utsumi, W., Funakoshi, K., Urakawa, S., Uchida, T., Katsura, T., Ohtaka, O., 1998. The postspinel phase boundary in Mg_2SiO_4 determined by in situ X-ray diffraction. Science 279, 1698-1700.

Ito, E., Katsura, T., 1989. A temperature profile of the mantle transition zone. Geophys. Res. Lett. 16, 425–428.

Ito, E., Takahashi, E., 1989. Postspinel Transformations in the system Mg_2SiO_4–Fe_2SiO_4 and some geophysical implications. J. Geophys. Res. 94, 10637–10646.

Jeanloz, R., Knittle, E., 1989. Density and composition of the lower mantle. Phil. Trans. R. Soc. Lond. 328, 377–389.

Kanzaki, M., Stebbins, J. F., Xue, X., 1991. Characterization of quenched high pressure phases in $CaSiO_3$ systemby X-ray and ^{29}Si NMR, Geophys. Res. Lett. 18, 463-466.

Kesson, S. E., Fiz Gerald, J. D., Shelley, J. M., 1998. Mineralogy and dynamics of a pyrolite lower mantle. Nature 393, 252–255.

Kubo, A., Akaogi, M., 2000. Post-garnet transitions in the system $Mg_4S_4O_{12}$–$Mg_3Al_2Si_3O_{12}$ up to 28 GPa: phase relations of garnet, ilmenite and perovskite. Phys. Earth Planet. Inter. 121, 85–102.

Kuroda, K., Irifune, T., Inoue, T., Nishiyama, N., Miyashita, M., Funakoshi, K., Utsumi, W., 2000. Determination of the phase boundary between ilmenite and perovskite in MgSiO3 by in situ X-ray diffraction and quench experiments. Phys. Chem. Miner. 27, 523-532.

Mao, H. K., Chen, L. C., Hemley, R. J., Jephcoat, A. P., Wu, Y., Bassett, W. A., 1989. Stability and equation of state of $CaSiO_3$-perovskite to 134 GPa. J. Geophys. Res. 94, 17889-17894.

Matsui, M., Parker, S. C., Leslie, M., 2000. The MD simulation of the equation of state of MgO: As a pressure calibration standard at high temperature and high pressure. Am.

Mineral. 85, 312-316.

Matsui, M., Nisiyama, N., 2002. Comparison between the Au and MgO pressure calibration standards at high temperature. Geophys. Res. Lett. 29, 10.1029/2001GL014161.

Nishiyama and Yagi, 2003. Phase relation and mineral chemistry in pyrolite to 2200°C under the lower mantle pressures and implications for dynamics of mantle plumes. J. Geophys. Res. in press.

Oguri, K., Funamori, N., Uchida, T., Miyajima, N., Yagi, T., Fujino, K., 2000. Post-garnet transition in a natural pyrope: a multi-anvil study based on in situ X-ray diffraction and transmission electron microscopy. Phys. Earth Planet. Inter. 122, 157–186.

O'Neill, B., Jeanloz, R., 1990. Experimental petrology of the lower mantle: a natural peridotite taken to 54 GPa. Geophys. Res. Lett. 10, 1477–1480.

Ringwood, A. E., 1966. The chemical composition and origin of the earth. in Advances in Earth Sciences, edited by P. Hurly, M. I. T. Press, pp287-356.

Ringwood, A. E., Major, A., 1971. Synthesis of majorite and other high pressure gernets and perovskites, Earth Planet. Sci. Lett. 12, 411–418.

Shim, S. -H., Duffy, T., Shen, G., 2000. The equation of state of CaSiO3 perovskite to 108 GPa at 300 K. Phys. Earth Planet. Inter. 120, 327–338.

Takahashi, E., Ito, E., 1987. Mineralogy of mantle peridotite along a model geotherm up to 700 km depth. in High-Pressure Research in Mineral physics, edited by M. H. Manghnani and Y. Syono, TERRAPUB/American Geophysical Union, Tokyo, pp427-437.

Tsuchiya, T., Kawamura, K., 2002. First-principles electronic thermal pressure of metal Au and Pt. Phys. Rev. B 66, 094115.

Utsumi, W., Funakoshi, K., Urakawa, S., Yamakata, M., Tsuji, K., Konishi, H., Shimomura, O., 1998. Spring-8 beamline for high pressure science with multi-anvil apparatus. Rev. High Pressure Sci. Technol. 7, 1484-1486.

Wang, Y., Weidner, D., Guyot, F., 1996. Thermal equation of state of $CaSiO_3$ perovskite. J.

Geophys. Res. 101, 661–672.

Wang, Y., Weidner, D., Zhang, J., Gwanmesia, G. D., Liebermann, R. C., 1998. Thermal equation of state of garnets along the pyrope-majorite join. Phys. Earth Planet. Inter. 105, 59–71.

Wood, B. J., Rubie, D. C., 1996. The effect of alumina on phase transformations at the 660-kilometer discontinuity from Fe-Mg partitioning experiments. Nature 273, 1522–1524.

Wood, B. J., 2000. Phase transformations and partitioning relations in peridotite under lower mantle conditions. Earth Planet. Sci. Lett. 174, 341–354.

Yagi, T., Funamori, N., 1996. Chemical composition of the lower mantle inferred from the equation of state of $MgSiO_3$ perovskite. Phil. Trans. R. Soc. Lond. 354, 1371–1384.

Figure captions

Fig. 1. A schematic illustration of the cell assembly used in the present in-situ X-ray diffraction experiments. 1, pressure medium (CoO-doped MgO); 2, pressure medium (ZrO2); 3, heater (WC+diamond); 4, electrode (Mo); 5, thermocouple ($W_{97}Re_3$-$W_{75}Re_{25}$); 6, sample capsule (MgO); 7, sample lid (Mo); 8, starting material (pyrolite); 9, pressure marker (MgO+Au).

Fig. 2. Examples of X-ray diffraction profiles of pyrolite at high pressure and temperature. (A) ringwoodite, (B) transitional, and (C) post-ringwoodite assemblage. Rw, $(Mg,Fe)_2SiO_4$ ringwoodite; Gt, majorite garnet; CPv, $CaSiO_3$-rich perovskite; MPv, $MgSiO_3$-rich perovskite; Mw, magnesiowüstite. MgO* : an X-ray diffraction peak of sample capsule of semi-sintered periclase.

Fig. 3. Parts of the X-ray diffraction profiles obtained at the ambient conditions. (A) the run product recovered from 23.5 GPa and 1600°C (S141), and (B) the run product recovered from 25.1 GPa and 1600°C. We see complete disappearance of the diffraction peaks of majorite garnet in (B), which suggests that the garnet-to-perovskite transition in pyrolite is complete at a pressure between 23.5 and 25.1 GPa at 1600°C.

Fig. 4. Phase relations in pyrolite at 1600°C determined on the basis of the results of in-situ X-ray diffraction experiments. Dashed lines are the phase boundaries between ringwoodite and transitional assemblage, between transitional and post-ringwoodite assemblage, which are drawn assuming that the Clapeyron slopes of these boundaries are the same as that of spinel to postspinel boundary in Mg_2SiO_4 (Ito and Takahashi, 1989; Irifune et al., 1998). A dash-dot line represents the phase boundary between the

post-ringwoodite and the lower mantle assemblages assuming that the Clapeyron slope is the same as that of the post-garnet transition in a natural pyrope (Oguri et al., 2000).

Fig. 5. A representative back-scattered electron image of the recovered sample (OS957; 22.5 GPa, 1600°C). Symbols used: MPv, $MgSiO_3$-rich perovskite; Mw, magnesiowüstite; CPv, $CaSiO_3$-rich perovskite; Gt, majorite garnet. A scale bar represents 5 μm.

Fig. 6. Al-content in Mg-perovskite vs. apparent partition coefficient for iron and magnesium between Mg-perovskite and magnesiowüstite at about 1600°C. Numbers beside symbols represent the experimental pressures. We see a non-linear relation between the Al-contents and the partition coefficients, which is in good agreement with the Fe-Mg partitioning behavior between Mg-perovskite and magnesiowüstite in a simpler MgO-FeO-Al_2O_3-SiO_2 system (Frost and Langenhorst, 2002).

Table 1 Experimental conditions and results of in-situ X-ray diffraction experiments (T=1600°C)

Run No.	Load, tonf	Time, min	Pressure, GPa	Phases present
S138	800	7	20.57(4)	Rw+Gt+CPv
		64	20.36(10)	Rw+Gt+CPv
		97	20.64(24)	Rw+Gt+CPv
S136	900	20	21.79(7)	Rw+MPv+Mw+Gt+CPv
		24	21.74(13)	Rw+MPv+Mw+Gt+CPv
		79	21.28(10)	Rw+Gt+CPv
S139	950	18	22.63(13)	MPv+Mw+Gt+CPv
		66	21.72(10)	Rw+MPv+Mw+Gt+CPv
		125	21.57(13)	Rw+MPv+Mw+Gt+CPv
S110	1000	9	23.36(12)	MPv+Mw+Gt+CPv
		37	22.79(29)	MPv+Mw+Gt+CPv
		67	23.11(23)	MPv+Mw+Gt+CPv
		127	22.72(36)	MPv+Mw+Gt+CPv
S137	1200	153	22.45(8)	MPv+Mw+Gt+CPv
		182	22.45(9)	MPv+Mw+Gt+CPv
		206	22.14(18)	MPv+Mw+Gt+CPv
S141*	1300	120	23.53(5)	MPv+Mw+Gt+CPv
S143*	1500	120	25.10(19)	MPv+Mw+CPv

Symbols used: Rw, ringwoodite; MPv, $MgSiO_3$-rich perovskite; Mw, magnesiowüstite; Gt, majorite garnet; CPv, $CaSiO_3$-rich perovskite.

* : Temperature was estimated using the power-temperature relation obtained from other runs.

Numbers in parentheses are estimated errors.

Pressure values except those in S141 and S143 were reported by Matsui and Nishiyama (2002), and were calculated based on volume fractions of MgO using an equation of state proposed by Matsui et al. (2000).

Table 2 Chemical compositions of the coexisting phases in the run product of OS957

	MPv	σ	Mw	σ	Gt	σ
SiO_2	56.19	1.19	0.39	0.22	53.53	1.14
TiO_2	0.27	0.29	0.03	0.05	0.16	0.13
Al_2O_3	2.80	0.62	0.32	0.08	8.60	1.85
Cr_2O_3	0.29	0.16	0.84	0.14	0.58	0.20
FeO	3.97	0.79	27.79	1.27	4.09	0.45
MgO	36.66	1.35	68.99	1.41	29.82	2.63
NiO	0.09	0.10	0.97	0.20	0.16	0.09
CaO	0.61	0.30	0.11	0.07	3.42	1.73
Na_2O	0.19	0.06	1.06	0.10	0.90	0.29
Total	101.06	1.60	100.50	1.46	101.25	0.92
No. of oxygens	3		1		12	
Si	0.953	0.009	0.003	0.002	3.656	0.067
Ti	0.003	0.004	0.000	0.000	0.008	0.007
Al	0.056	0.013	0.003	0.001	0.692	0.150
Cr	0.004	0.002	0.005	0.001	0.031	0.011
Fe	0.056	0.012	0.178	0.008	0.233	0.026
Mg	0.926	0.024	0.786	0.006	3.035	0.251
Ni	0.001	0.001	0.006	0.001	0.009	0.005
Ca	0.011	0.006	0.001	0.001	0.251	0.129
Na	0.006	0.002	0.016	0.001	0.119	0.038
Sum	2.017	0.008	1.001	0.002	8.034	0.041
Mg*	0.943	0.012	0.816	0.009	0.929	0.008

Symbols used: MPv, $MgSiO_3$-rich perovskite; Mw, magnesiowüstite; Gt, majorite garnet.

Mg* = Mg/(Mg+Fe)

Chemical composition data represent averages of ten analyses, and σ represents the one standard deviation.

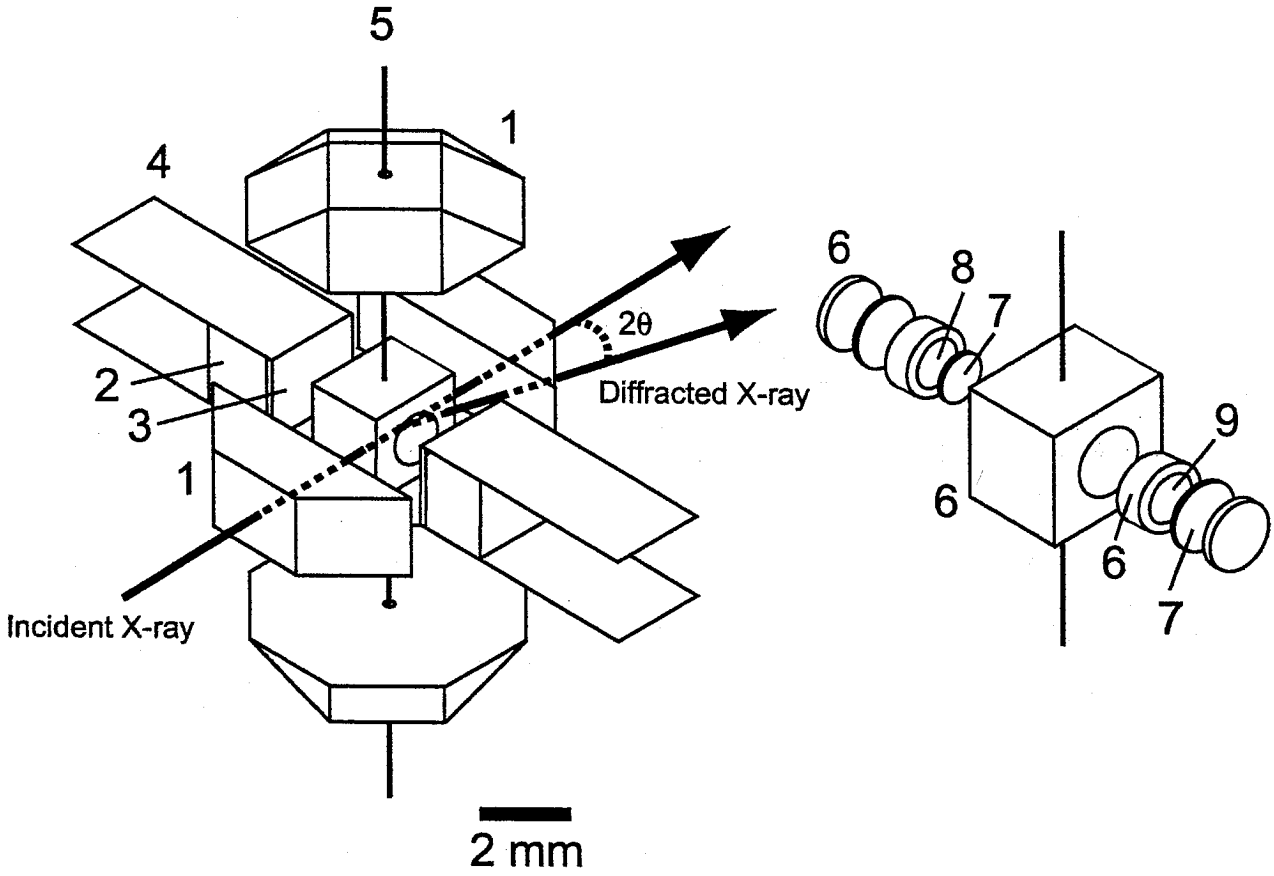

Fig. 1

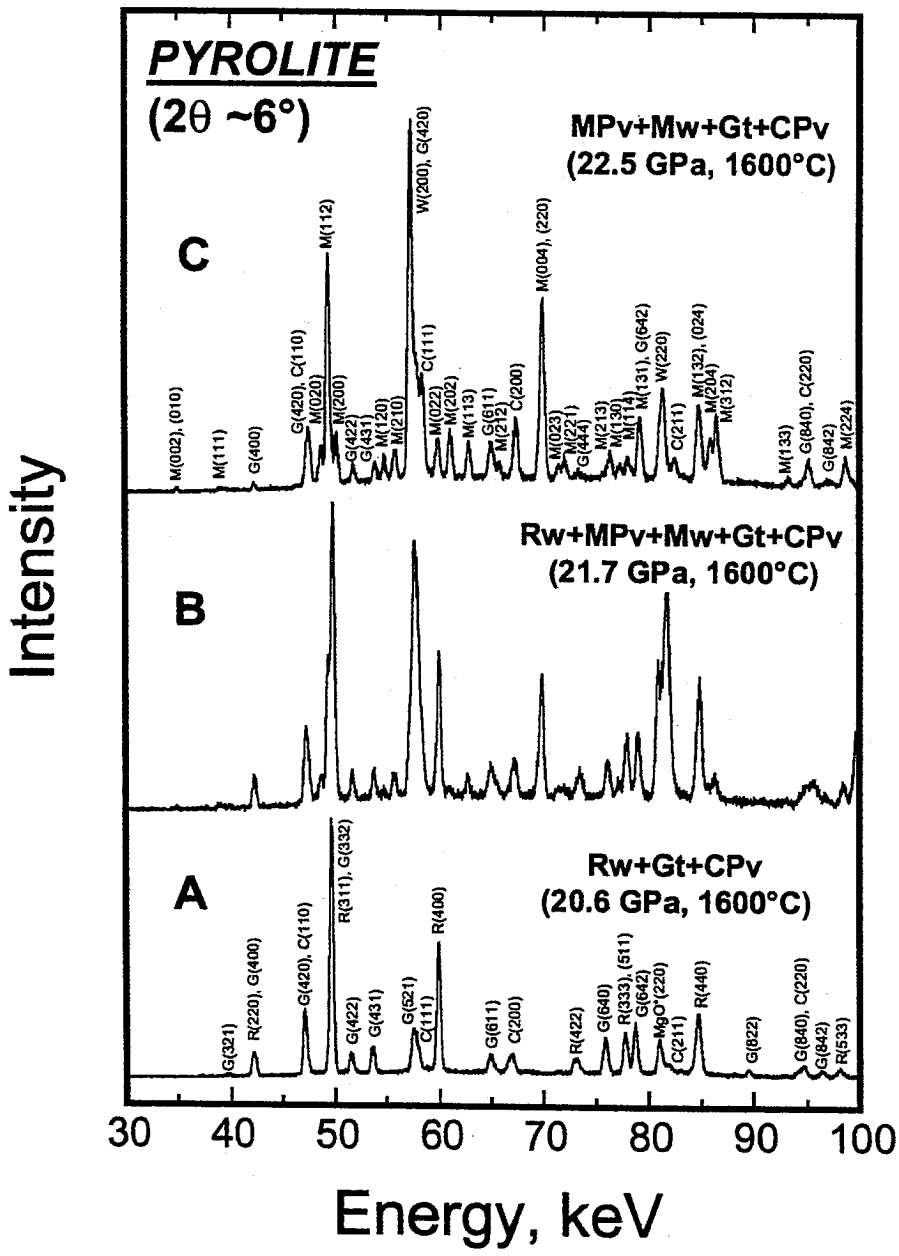
PYROLITE
(2θ ~6°)
MPv+Mw+Gt+CPv
(22.5 GPa, 1600°C)
C
M(002), (010)
M(111)
G(400)
G(420), C(110)
M(020)
M(112)
M(200)
G(422)
G(431)
M(120)
M(210)
W(200), G(420)
C(111)
M(022)
M(202)
M(113)
G(611)
M(212)
C(200)
M(004), (220)
M(023)
M(221)
G(444)
M(213)
M(130)
M(114)
M(131), G(642)
W(220)
C(211)
M(132), (024)
M(204)
M(312)
M(133)
G(840), C(220)
G(842)
M(224)
Rw+MPv+Mw+Gt+CPv
(21.7 GPa, 1600°C)
B
Rw+Gt+CPv
(20.6 GPa, 1600°C)
A
G(321)
R(220), G(400)
G(420), C(110)
R(311), G(332)
G(422)
G(431)
G(521)
C(111)
R(400)
G(611)
C(200)
R(422)
G(640)
R(333), (511)
G(642)
MgO*(220)
C(211)
R(440)
G(822)
G(840), C(220)
G(842)
R(533)
30
40
50
60
70
80
90
100
Intensity
Energy, keV

Fig. 2

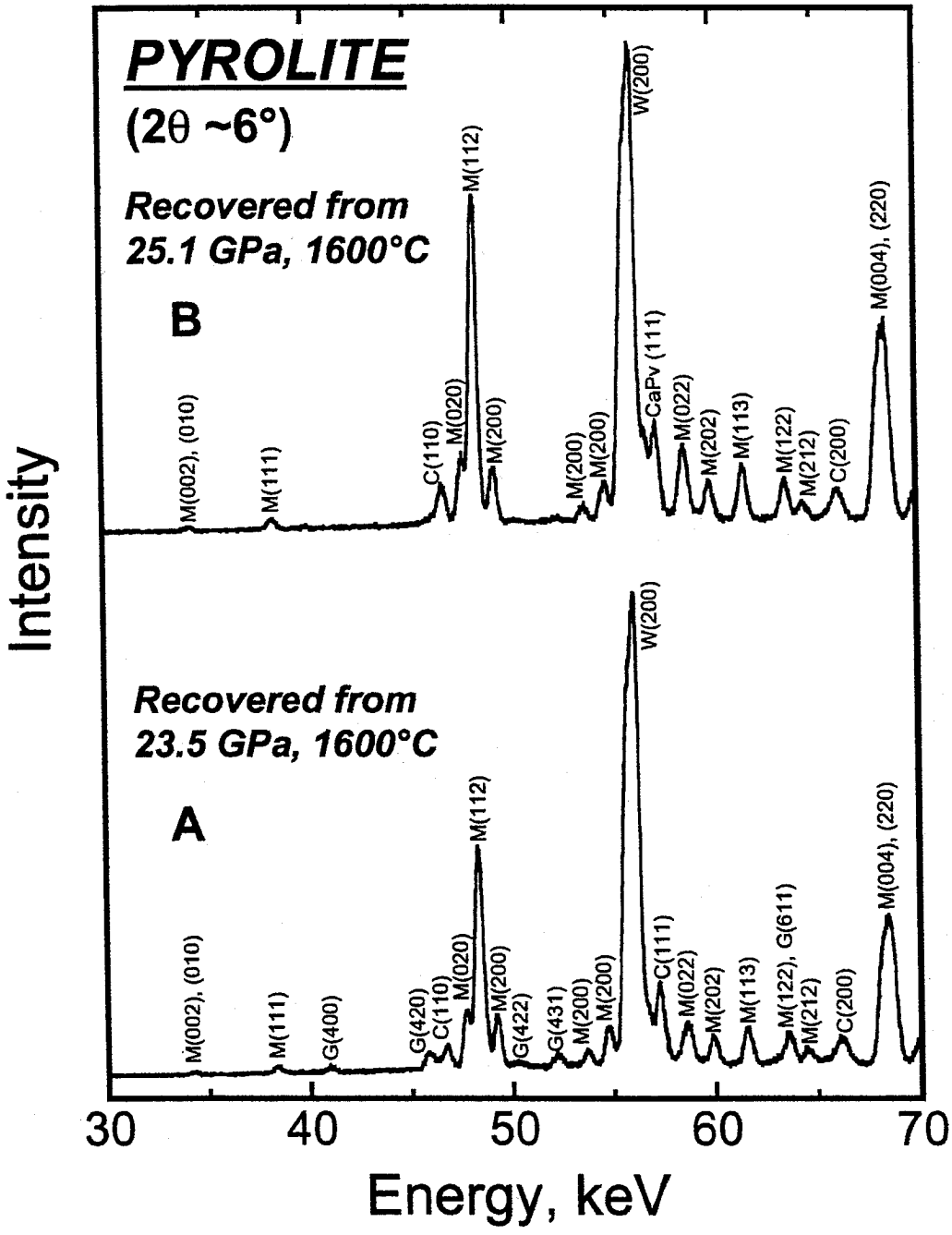
PYROLITE
(2θ ~6°)
Recovered from
25.1 GPa, 1600°C
B
M(002), (010)
M(111)
C(110)
M(020)
M(112)
M(200)
M(200)
M(200)
W(200)
CaPv (111)
M(022)
M(202)
M(113)
M(122)
M(212)
C(200)
M(004), (220)
Recovered from
23.5 GPa, 1600°C
A
M(002), (010)
M(111)
G(400)
G(420)
C(110)
M(020)
M(112)
M(200)
G(422)
G(431)
M(200)
M(200)
W(200)
C(111)
M(022)
M(202)
M(113)
M(122), G(611)
M(212)
C(200)
M(004), (220)
Intensity
30
40
50
60
70
Energy, keV

Fig. 3

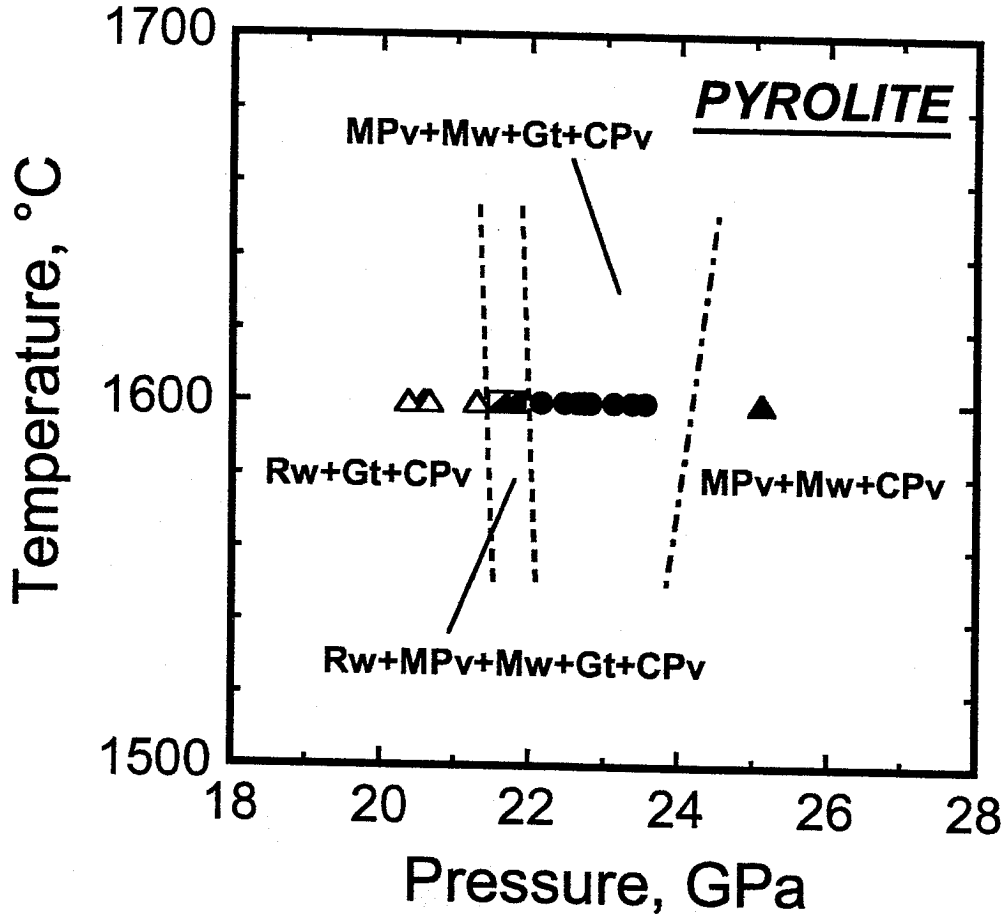
1700
1600
1500
Temperature, °C
18
20
22
24
26
28
Pressure, GPa
PYROLITE
MPv+Mw+Gt+CPv
Rw+Gt+CPv
MPv+Mw+CPv
Rw+MPv+Mw+Gt+CPv

Fig. 4

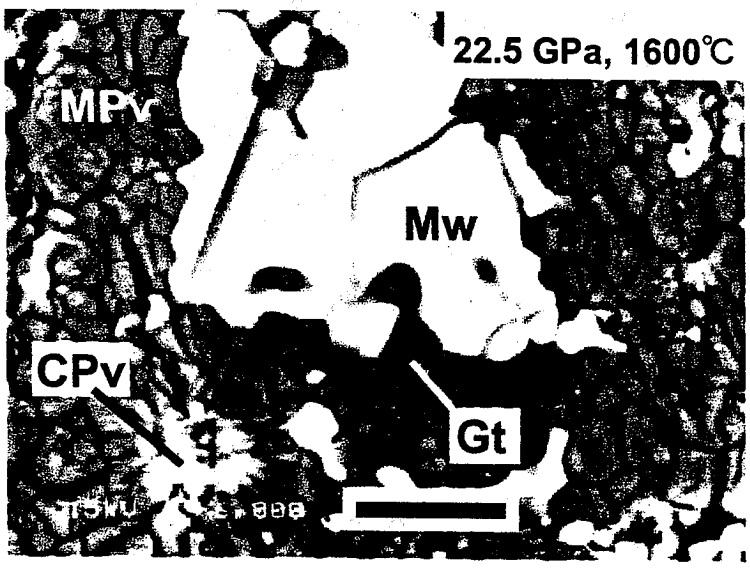

Fig. 5

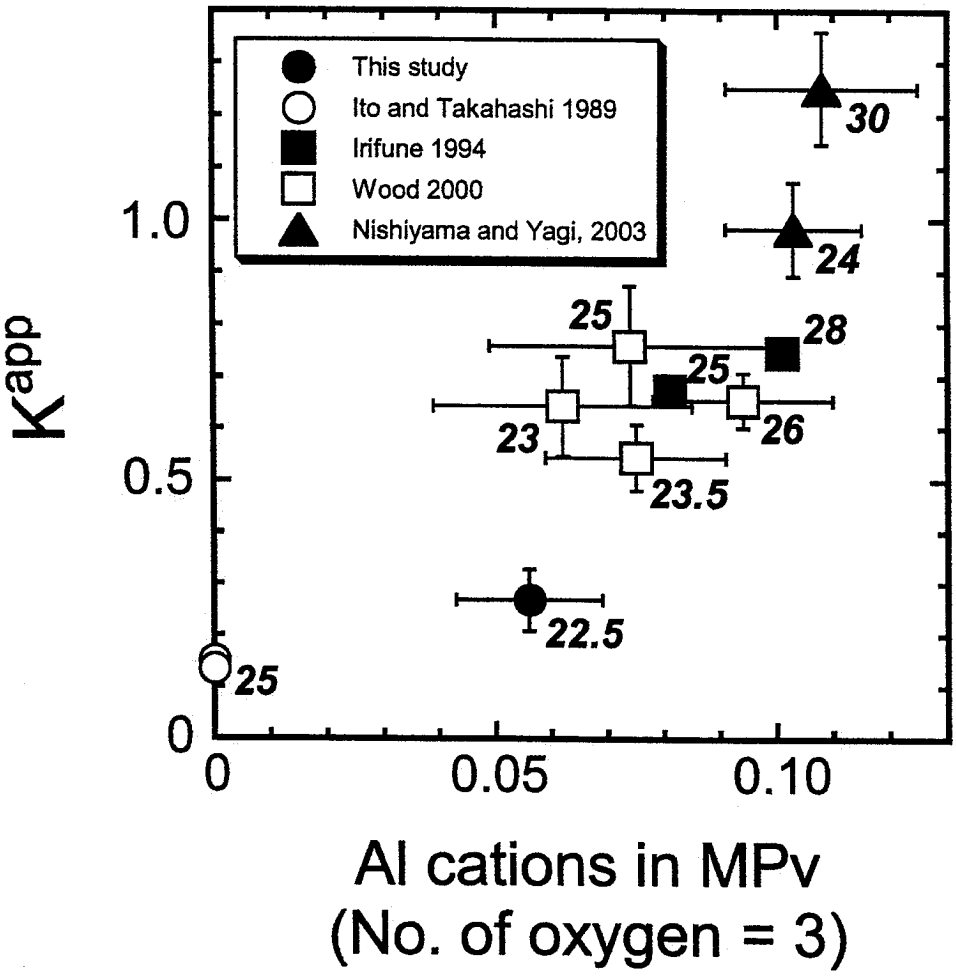
This study
Ito and Takahashi 1989
Irifune 1994
Wood 2000
Nishiyama and Yagi, 2003
30
24
25
28
25
26
23
23.5
22.5
25
1.0
0.5
0
0
0.05
0.10
K^{app}
Al cations in MPv
(No. of oxygen = 3)

Fig. 6